Hindawi
Science and Technology of Nuclear Installations
Volume 2022, Article ID 1758382, 12 pages
https://doi.org/10.1155/2022/1758382

Research Article

Numerical Study of Unsteady Pressure Fluctuation at Impeller Outlet of a Centrifugal Pump

Xiaojie Ma, Lulu Zheng, Jinglei Qu, and Mengmeng Wang

Faculty of Mechanical Engineering, Henan Institute of Technology, Xinxiang, Henan 453003, China

Correspondence should be addressed to Lulu Zheng; zhengll012@163.com

Received 15 February 2022; Accepted 10 August 2022; Published 30 August 2022

Academic Editor: Leon Cizelj

Intense fluid-dynamic interaction at the impeller outlet strongly affects the unsteady flow and pressure stability within the centrifugal pump. In order to have a better understanding of the pressure fluctuation of centrifugal pumps, a numerical calculation is carried out by using the RNG k-epsilon turbulence model under various flow rates. The numerical calculation results are compared with the experimental results in order to verify the reliability of the calculation model. The amplitude and frequency distribution of pressure fluctuation at the impeller outlet is obtained and analyzed in the time and frequency domain. The research results show that the blade passing frequency is the dominant frequency of the pressure fluctuation. And the pressure fluctuation is a periodic fluctuation. As the flow rate decreases, the periodicity of the pressure fluctuation decreases. Besides, the amplitude and intensity of pressure fluctuation are closely related to flow rate and spatial location. At the low flow rate, the amplitude of pressure fluctuation in the time domain and frequency domain is enlarged greatly, especially near the tongue region. The pressure difference distribution on both sides of the blade surface is extremely uneven, and the pressure changes significantly.

1. Introduction

As an important energy conversion equipment, centrifugal pumps have been widely used in industrial processes and modern engineering. Pressure fluctuation is a complex phenomenon of fluid dynamics in centrifugal pumps, which affects the stable operation of centrifugal pumps and the life of equipment [1–7]. Strong rotor-stator interaction is the main source of large pressure fluctuation, which has a great impact on the stable and safe operation of the centrifugal pump. In the designing process of the pumps, reducing the pressure fluctuation inside the centrifugal pump should be considered. The comprehensive understanding of unsteady pressure fluctuation lays a foundation for further reducing the pressure fluctuation intensity of the pump.

In recent years, due to the engineering needs of centrifugal pumps, more and more attention has been paid to pressure fluctuation characteristics [8–10]. Gonzalez et al. [11] studied the unsteady flow effects due to impeller-volute interaction in a centrifugal pump and found that the pressure fluctuation level increases largely at off-design flow rates. Bai et al. [12] studied the pressure fluctuation and unsteady flow in a centrifugal pump. Results show that the pressure fluctuation amplitude in the diffuser increases gradually with the increase of the diffuser vanes numbers. Wang et al. [13] analyzed the unsteady pressure fluctuation in a multistage centrifugal pump with the whole flow field and revealed the main factors which have a large effect on the intensity of the pressure fluctuation within the pump. Liu et al. [14–16] investigated the pressure characteristics and internal flow characteristics of the pump with clearance.

The pressure fluctuation within the pump has been investigated by using experimental and numerical methods [9, 17, 18]. Spence and Amaral-Teixeira [19] studied the pressure fluctuation in a centrifugal pump by using numerical methods under different flow rates. Jin et al. [20] investigated the transient characteristics in a double-suction centrifugal pump during the starting period by numerical simulation and experimental validation.

Research on reducing the intensity of pressure fluctuation has also been carried out by many scholars. Zhang et al. [21] studied the unsteady pressure fluctuation distribution in

a centrifugal pump with a slope volute and found that a slope volute pump significantly reduces the intensity of pressure fluctuation. Gao et al. [22] studied the effect of the blade trailing edge profile on the performance and unsteady pressure fluctuation in a centrifugal pump. The results show that the ellipse on the pressure side and ellipse on both sides' profiles contribute significantly to the reduction of pressure fluctuation. Gao et al. [23] studied the pressure fluctuation distribution in a centrifugal pump with different cutting blades. It is found from multiple comparisons that an appropriate cut angle can effectively reduce the intensity of the pressure pulsation in the pump. Song et al. [8] analyzed the effect of impeller arrangement on pressure fluctuation in a double-suction centrifugal pump. Results show that a suitable impeller arrangement can improve pump performance and reduce the intensity of pressure fluctuation.

While numerous studies have investigated the pressure fluctuation and unsteady characteristics in different kinds of pumps, the pressure fluctuation characteristics at the impeller outlet still need further investigation. So, in the present work, the unsteady pressure fluctuation characteristics at the impeller outlet are carried out in a centrifugal pump under various flow rates. The numerical calculation results are compared with the experimental data to verify the accuracy of the calculation results. The amplitudes of pressure fluctuations at monitoring points under various flow rates in the time domain and frequency domain are studied and analyzed in detail.

2. Design Method

2.1. Parameters of the Centrifugal Pump. The centrifugal pump studied in the present work is a single-stage single-suction centrifugal pump. Figure 1 shows the computational domain of the centrifugal pump which consists of four computational domains: impeller, volute, inlet, and outlet. The numerical calculations are carried out with this computation domain under various flow rates. The parameters of the pump are listed in Table 1. The flow rate and the pressure head at the design flow rate are $Q_d = 551\ \mathrm{m}^3/\mathrm{h}$ and $H_d = 25\ \mathrm{m}$, respectively.

2.2. Independence Verification of Mesh Density. Mesh quality has a great influence on the accuracy of numerical calculation. The structured mesh has better convergent characteristics in the numerical calculation of the pump than the unstructured mesh. Besides, the structured mesh has significant advantages in dealing with key areas such as the volute tongue. Thus, the hexahedral mesh is used in the computation domain of the centrifugal pump. Structure mesh cells are generated in order to achieve accurate unsteady flow structures and pressure properties. The flow field near the wall has a large variation in velocity and pressure, so the mesh near the solid surface was mainly refined in order to ensure the calculation accuracy.

Before the numerical calculation, the mesh independence test was carried out. The nondimensional pressure head coefficient is defined as follows:

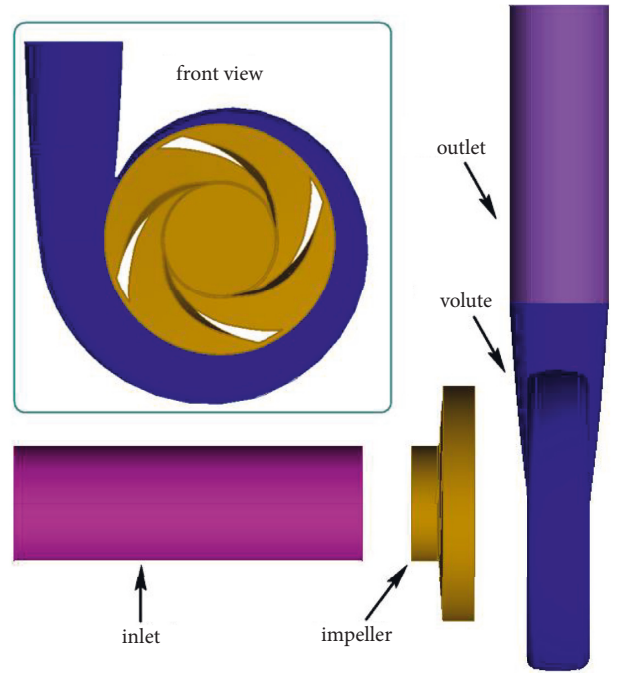

Figure 1: 3D model of the centrifugal pump.

Table 1: Geometric parameters of centrifugal pump.

Parameters	Symbol	Value
Inlet diameter of impeller	D_0	230 mm
Outlet diameter of impeller	D_1	450 mm
Design flow rate	Q_d	551 m^3/h
Design pressure head	H	25 m
Rotating speed	n	980 rpm
Blades number	Z	4

Table 2: Mesh independence test.

Case	Mesh (million)	φ
1	2.38	0.005378
2	3.34	0.005305
3	5.71	0.005263
4	6.99	0.005257
5	11.06	0.005253

$$\varphi = gH/\left(n^2 r^2\right), \tag{1}$$

where g stands for gravity, H stands for the pressure head, n stands for the rotating speed and r stands for the outer radius of the impeller. Five sets of meshes ranging from 2.38 million to 11.06 million were applied in the mesh independence test. The results of pressure head coefficient under different mesh numbers are shown in Table 2.

When the number of elements increases to 5.71 million, there is limited influence on the centrifugal pump head coefficient. Therefore, considering the factors of computing resources and calculation accuracy, the case with 5.71 million elements is selected for the final calculation. The mesh is fine enough to satisfy $y^+ < 200$ near the wall. This

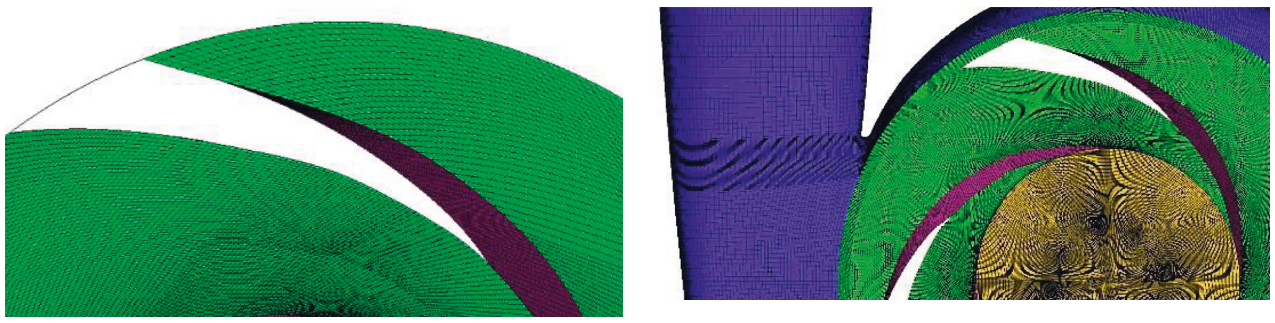

(a) (b)

Figure 2: Mesh detail of the pump. (a) Impeller and (b) pump.

mesh size can give the correct result of pump performance and allow the analysis of the details of the main flow patterns involved such as flow separation and secondary flow. The mesh detail of the impeller and volute is presented in Figure 2.

2.3. Numerical Methods. The Governing equation in this study is the unsteady three-dimensional incompressible Reynolds-averaged Navier–Stokes equations. The numerical calculations are conducted by using the commercial CFD code of ANSYS-Fluent 16.0. The medium used for numerical calculations and experiments is water. RNG k-ε turbulence model is used in the numerical calculation, which is also applied in many studies [24–27]. The finite volume method (FVM) is used to solve the system and the coupling between velocity and pressure is obtained by the SIMPLE algorithm. The velocity inlet is selected at the inlet of the duct. Neumann boundary condition is applied at the outlet of the domain for velocity and the pressure is given at the outlet. No slip wall is imposed on the solid walls.

The transient flow characteristics in the centrifugal pump are obtained by two steps of calculation, namely, steady calculation, and unsteady calculation. First of all, the steady numerical calculation result is first obtained by using the multiple frames of reference (MRF) method. Secondly, the calculation data of steady numerical simulation in the pump is taken as the initial condition of the unsteady computation by using the sliding mesh model. For each impeller revolution, the calculation is performed in a time sequence of 360 time steps. The time step is set as $\Delta t = 1.7 \times 10^{-4}$ s, which is corresponding to one rotation degree of the impeller, in order to obtain enough resolution of unsteady flow rates.

2.4. Location of Pressure Monitoring Points. Strong pressure fluctuation induced by rotor-stator interaction has a great impact on the centrifugal pump. In order to obtain the pressure fluctuation characteristic of the pump at the impeller outlet, eight points were equally distributed, as shown in Figure 3. For point 1, the angle with the horizontal axis is 45 degrees, and the angle between two adjacent points is 45 degrees.

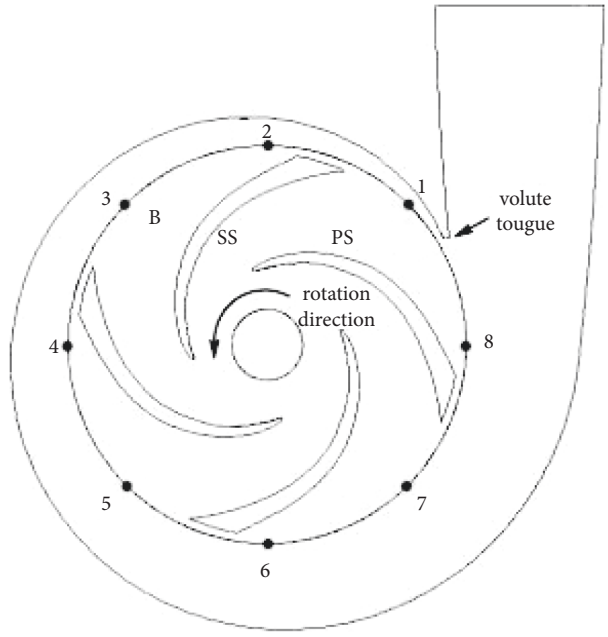

Figure 3: Distributions of monitoring points.

3. Results and Discussions

3.1. Validation of the Numerical Simulation. Figure 4 shows the comparison between the numerical calculation results of the centrifugal pump and the experimental results [28]. It is discovered that the head curve of numerical calculation is in good agreement with the experimental data overall. The maximum of the relative error is within 5%. At the design flow rate, the relative error between the experimental data and the predicted flow rate is about 2.5%. In total, the small difference in head performance illustrates that the calculation model, mesh system, and boundary conditions in the present calculation are valid to predict the centrifugal pump performances.

Figure 5 shows the distribution of head and velocity at the pump outlet versus the time. It is observed that the distribution of the pump head shows periodic fluctuations, and it shows a tendency to stabilize. However, the velocity distribution at the pump outlet does not show a uniform distribution trend. The velocity fluctuates greatly and

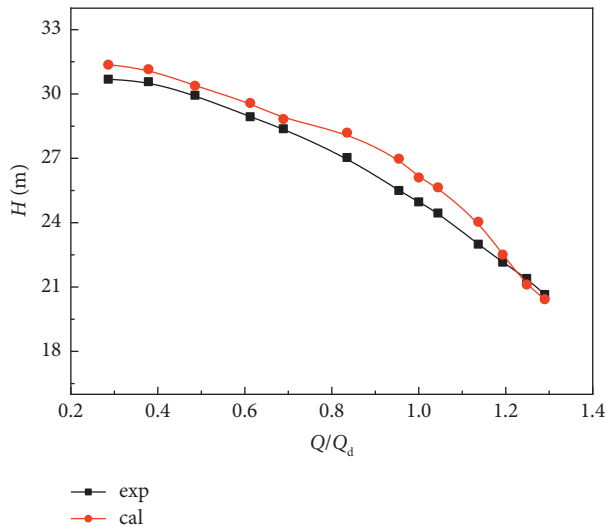

Figure 4: Head curve of the pump.

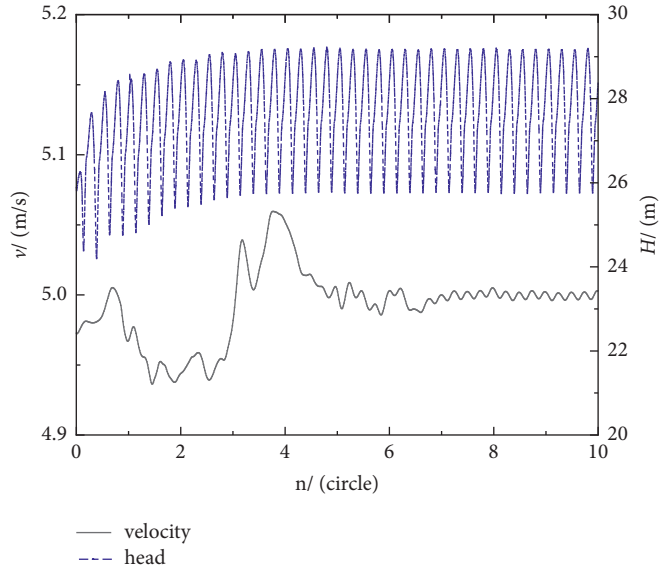

Figure 5: Distribution of head and outlet velocity with respect to impeller rotations.

presents an irregular trend after the impeller rotates. It is noticed that the velocity reaches its steady state after 8 circles. Thus, the analysis of pressure fluctuation is carried out after this time.

3.2. Unsteady Pressure Fluctuation at Impeller Outlet. The pressure coefficient is used to describe the distribution of pressure fluctuation which is defined as follows:

$$c_p = \frac{p - \overline{p}}{0.5\rho u^2}, \tag{2}$$

where p stands for static pressure,$\overline{p}$ stands for time average static pressures of the probes, and u stands for impeller circumferential velocity.

At the initial position, the tongue is corresponding to the middle region of the impeller outlet, as is shown in Figure 3. Figure 6 presents the pressure fluctuation and frequency spectra at selected monitoring points at the design flow rate. The pressure fluctuation at each monitoring point is closely related to the relative position between blades and volute tongue [29]. As can be seen from Figure 6(a), the pressure fluctuation at the monitoring point has an obvious periodic fluctuation rule. The pressure fluctuation at $p1$ near the tongue is relatively larger. Besides, it is found that the distribution of pressure fluctuation can be roughly divided into two categories, which are presented in Figure 6(a). The two types of classification are mainly based on the position of the peaks and valleys in the pressure fluctuation distribution, which is related to the blades' number and the relative

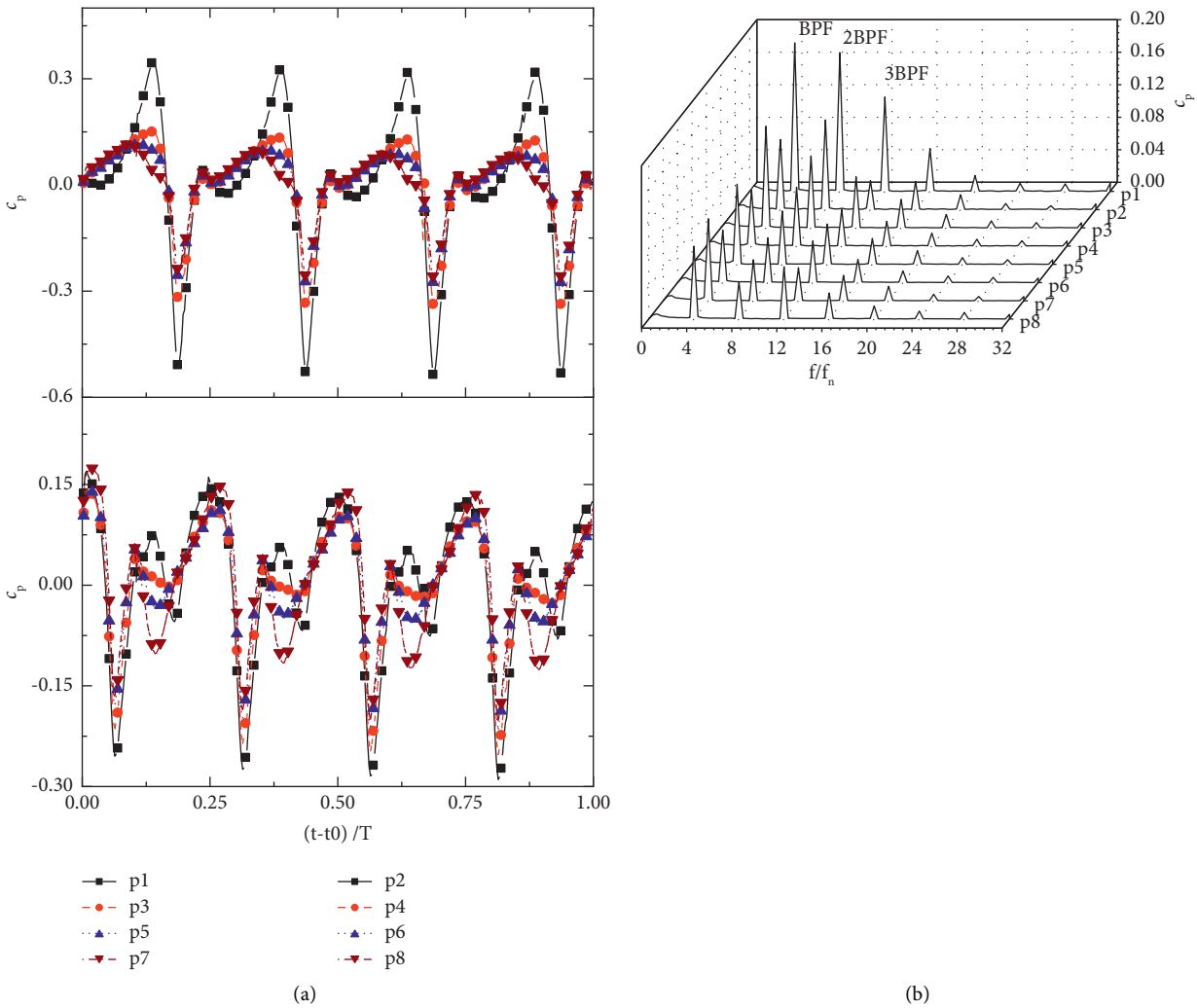

FIGURE 6: Pressure fluctuation and frequency spectra distribution at selected monitoring points. (a) Pressure fluctuation and (b) pressure spectra.

position between the impeller and volute tongue. The frequency and amplitude of the pressure fluctuation are obtained by fast Fourier transformation (FFT), which is presented in Figure 6(b). The f_n stands for impeller rotating frequency. It is found that the main pressure fluctuation components possess the blade passing frequency (f_{BPF}) and its harmonic frequencies.

As Figure 7 shows, the pressure fluctuation components at f_{BPF}. It is observed that the distribution of pressure spectra at f_{BPF} shows a trend of wavy decline, in general. The maximum value is obtained at $p1$, which locates near the volute tongue. As the monitoring points move away from the volute tongue, the pressure amplitudes decrease due to the weakening of the pressure fluctuation intensity. The variation between each of the three monitoring points shows a completely opposite distribution trend, as shown by the blue arrow in Figure 7. The pressure spectra at f_{BPF} show some degree of modulation, which is characterized by the four peaks and valleys. This modulation pattern is closely

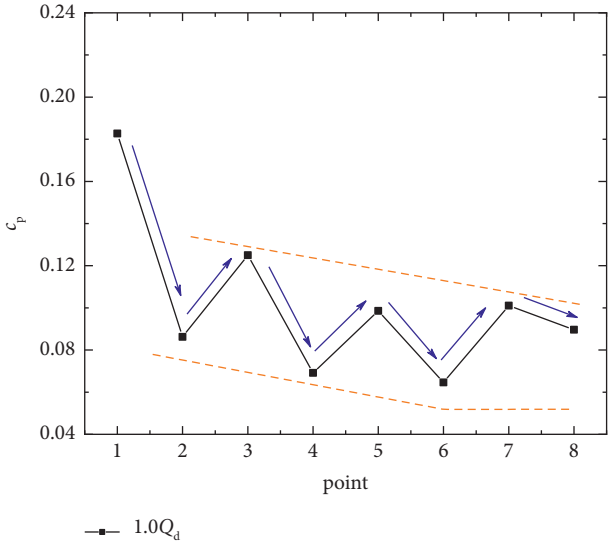

FIGURE 7: Distribution of pressure spectra at f_{BPF}.

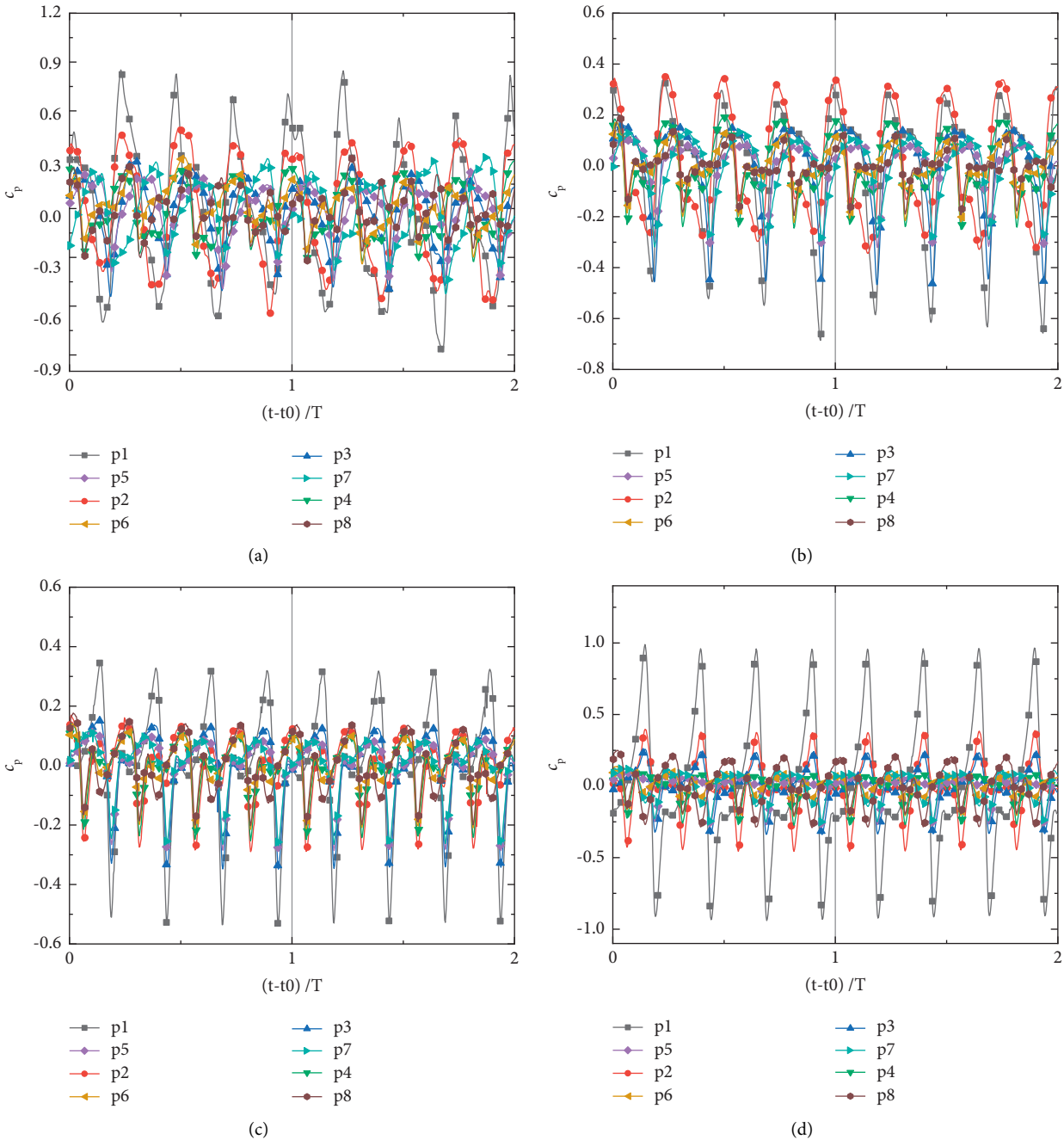

Figure 8: Unsteady pressure fluctuations at monitoring points. (a) $0.4Q_d$, (b) $0.7Q_d$, (c) $1.0Q_d$, (d) $1.3Q_d$.

related to the hydraulic disturbances and rotor-stator interaction inside the pump [30–32].

3.3. Influence of Flow Rate on Pressure Fluctuation Distribution. Figure 8 shows the pressure fluctuation in the time domain at different flow rates in two impeller revolutions. It is noticed that the pressure fluctuation distribution of monitoring points presents a periodic distribution. As is shown in Figure 8, there are four distinct peaks and valleys for each monitoring point in one impeller revolution, which is corresponding to four impeller blades. It is obvious that the pressure fluctuation characteristics show significant differences at different flow rates. At $0.4Q_d$, the pressure fluctuation signals are irregular and nonuniform. The pressure signal fluctuates largely at $p1$, which locates near the volute tongue. At $0.7Q_d$, the pressure fluctuation shows certain regularity, and the range of pressure fluctuation is decreased to a certain extent. At $1.0Q_d$, the pressure fluctuation distribution is quite regular and pressure fluctuation amplitude in the time domain achieves its minimum value. The pressure signal changes periodically overtime at the

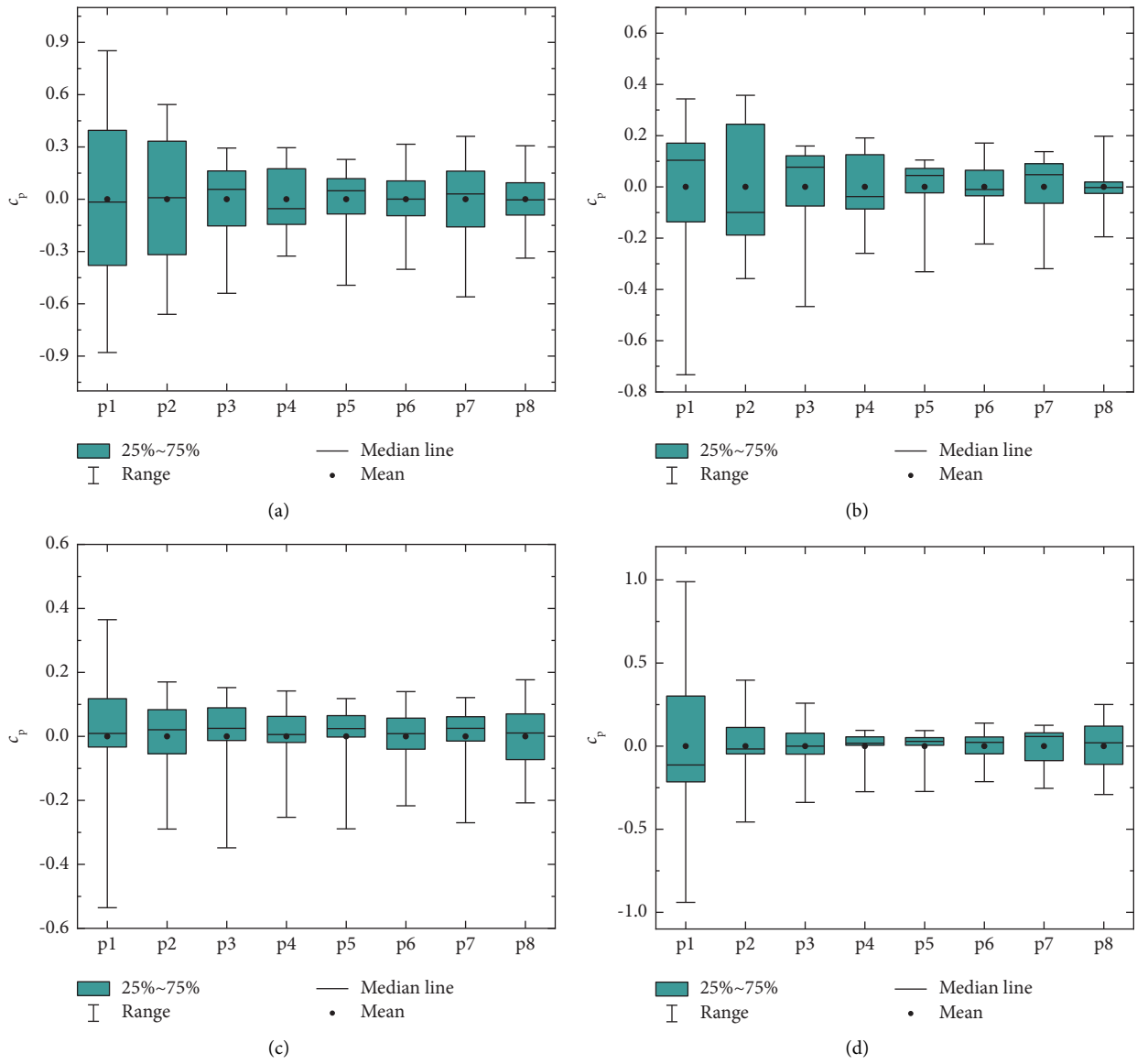

Figure 9: Amplitude and the average value of monitoring points under different flow rates. (a) $0.4Q_d$, (b) $0.7Q_d$, (c) $1.0Q_d$, (d) $1.3Q_d$.

monitoring points. As the flow rate increases to $1.3Q_d$, the pressure fluctuation amplitude in the time domain increases obviously, especially at $p1$.

Figure 8 mainly presents the distribution regulation of pressure fluctuation over time. However, the data is mainly about qualitative analysis of pressure fluctuation distribution. Therefore, the average value and distribution range of pressure fluctuation at each measuring point at different flow rates are analyzed in detail. Figure 9 shows data such as the amplitude and average value of the pressure fluctuation range at each point under different flow rates. Because of the wide range of pressure fluctuations, the average pressure of each measuring point does not change significantly with the space and flow rate, so it is especially given in Figure 10. The range of the pressure fluctuation stands for the amplitude of the pressure fluctuation. At $0.4Q_d$, the range of pressure fluctuation at monitoring points is relatively large, which reveals the strong unsteady pressure fluctuation. In general, the pressure fluctuation range decreases from $p1$ to $p5$ region and increases to $p7$ then decrease to $p8$. The maximum pressure fluctuation range is obtained at $p1$, which was affected by the volute tongue, while the minimum value is obtained at approximately $p5$. Distribution of pressure fluctuation range indicates pressure fluctuation strength at monitoring $p1$ and $p2$ is stronger than at other points.

Internal complex unsteady flow is the main reason for the large pressure fluctuation. As the flow rate increases to $0.7Q_d$, the pressure distribution is similar to $0.4Q_d$, while the pressure fluctuation range at the monitoring points is decreased in a small scale. At the design flow rate, the maximum pressure at monitoring points is almost the same, except for $p1$. At $1.3Q_d$, the pressure fluctuation range of the remote tongue measuring point does not change much, but the pressure near the tongue measuring point increases to

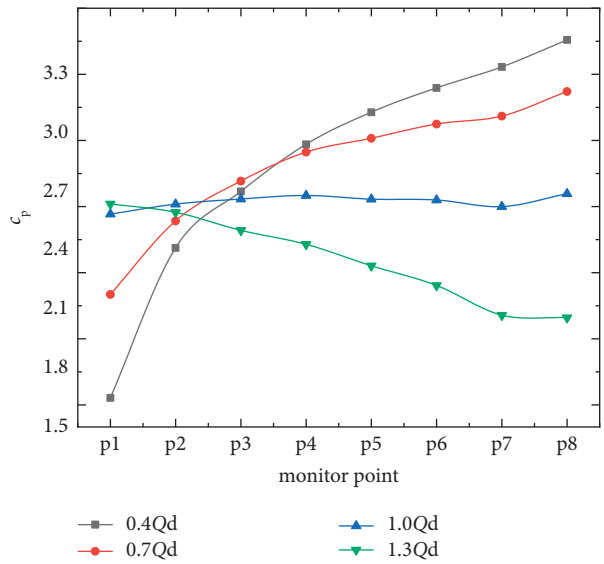

Figure 10: Average pressure distribution under different flow rates.

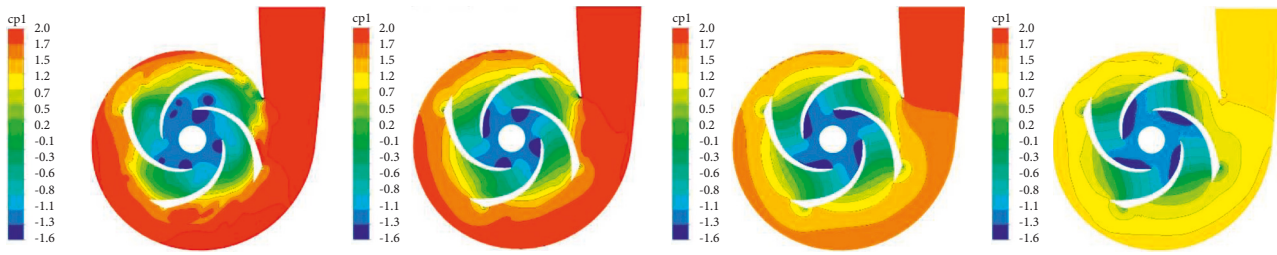

Figure 11: Pressure coefficient distributions on the center plane. (a) $0.4Q_d$, (b) $0.7Q_d$, (c) $1.0Q_d$, and (d) $1.3Q_d$.

varying degrees. The increase of $p1$ was most significant near the tongue, indicating that the rotor-stator interaction was the most significant near the tongue.

As Figure 10 shows the average pressure distribution at different flow rates. At $0.4Q_d$, the average pressure at the monitoring points increases obviously from $p1$ to $p8$. The pressure value increases from $p1$ along the counter-clockwise direction, which is in accord with the supercharged principle of the pump volute. The minimum average pressure is achieved at $p1$, and it is obviously lower than other points. At $0.7Q_d$, the average pressure increases gently from $p1$ along the counter-clockwise direction. At $1.0Q_d$, the average pressure value of the monitoring points is almost the same, which reveals the uniform pressure distribution at the design flow rate. At $1.3Q_d$, the average pressure of the monitoring points decreased from $p1$ to $p8$, which is different from other flow rates. The volute has the function of collecting fluid and is also an energy conversion device. Along the spiral direction of the volute, the cross-sectional area of the volute flow channel gradually expands, so the high-speed fluid thrown out by the impeller can be gradually decelerated, and the kinetic energy can be effectively converted into static pressure energy. The increase in flow rate causes the movement of the low-pressure area in the flow channel towards the inlet of the volute, as shown in Figure 11(d). In addition, the unsteady flow and the large flow rate affect the conversion of kinetic energy into static pressure by the volute to some extent, thus causing the distribution of the impeller outlet pressure under $1.3Q_d$.

3.4. Pressure Fluctuation in Frequency Domain. As is shown in Figure 12, the pressure fluctuation in the frequency domain at different flow rates shows discrete spectral characteristics. It was found that the dominant frequency is f_{BPF} and its multiples. The pressure fluctuation amplitude shows a decaying trend in the frequency domain. Evident peaks at harmonic frequency $3f_{BPF}$ could be identified. However, its amplitude has been greatly reduced.

Pressure fluctuation amplitude in the frequency domain is relatively small at $1.0Q_d$, which reveals a good internal flow situation. However, pressure fluctuation amplitude in the frequency domain is increased obviously at off-design flow rates, especially at the small flow rate. The amplitude of pressure fluctuation at different monitoring points also varies greatly. In general, the maximum amplitude of pressure fluctuation in the frequency domain is obtained at $p1$, which is located near the tongue. The amplitude of pressure fluctuation in the frequency domain is decreased from $p1$ along the impeller rotation direction. With the increase of the flow rate, the pressure fluctuation amplitude

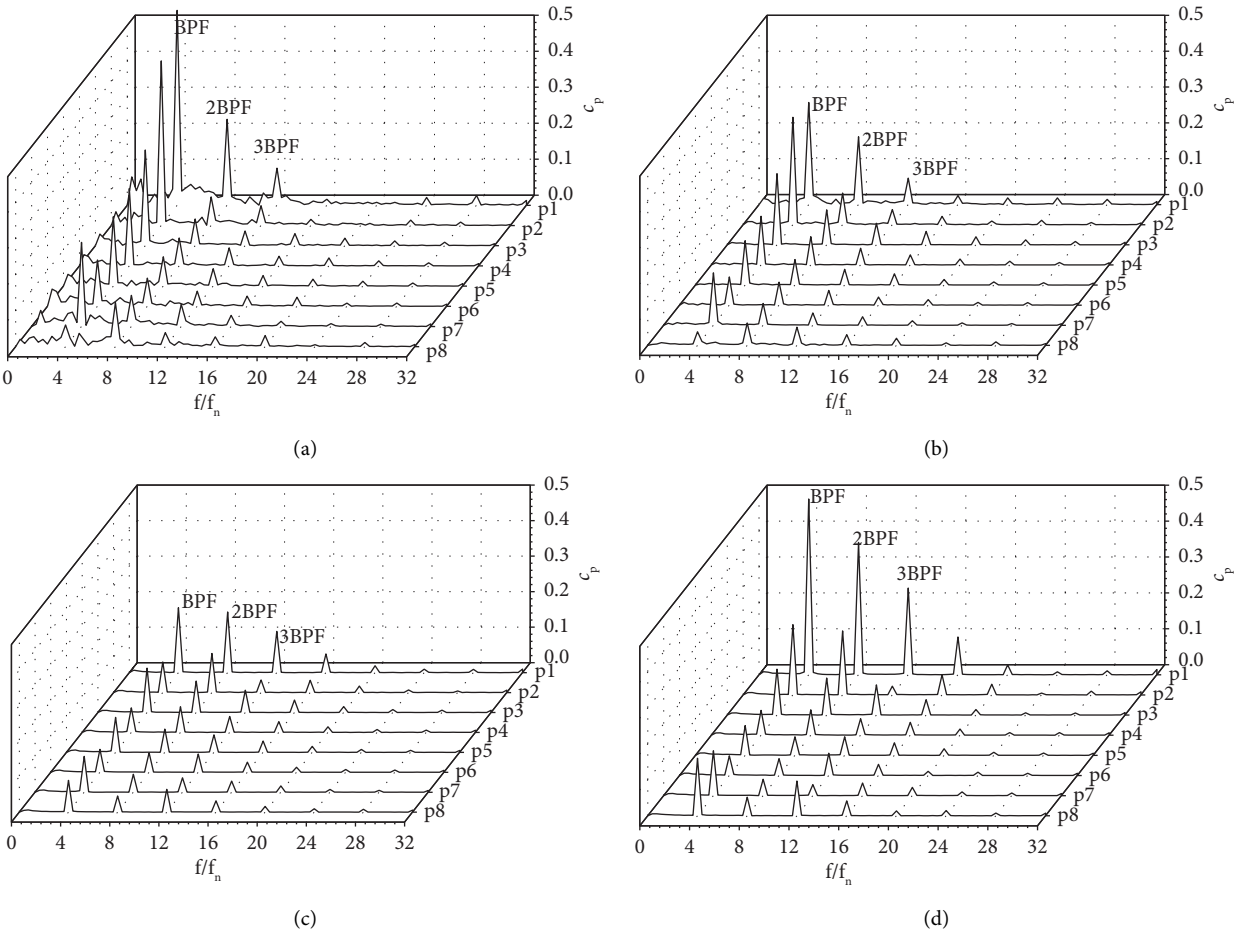

Figure 12: Pressure fluctuation amplitude in the frequency domain. (a) $0.4Q_d$, (b) $0.7Q_d$, (c) $1.0Q_d$, (d) $1.3Q_d$.

in the frequency domain first decreases and then increases and the minimum of which was obtained at $1.0Q_d$.

Figure 13 shows the amplitude of pressure fluctuation under f_{BPF} and $2f_{\mathrm{BPF}}$ at the monitoring points. It was found in Figure 13(a) that, with the increase of the flow rate, the amplitude of pressure fluctuation decreases, and its minimum value achieves at the design flow rate. As the flow rate increased from $1.0Q_d$ to $1.3Q_d$, the amplitude of the pressure fluctuation shows an increasing trend. The amplitude of pressure is relatively large at the partial flow rate, especially at $0.4Q_d$. For large flow rates, the amplitude distribution is almost consistent with the design flow rate, except for the measuring points near the tongue. In Figure 13(b), the pressure amplitude at the monitoring points has a similar distribution tendency. The pressure fluctuation amplitude at the measuring point near the tongue is relatively large. The amplitude of pressure fluctuation is relatively large from $p1$ to $p3$ at $1.3Q_d$. While the amplitude of pressure fluctuation is relatively large from $p5$ to $p8$ under the $0.4Q_d$ flow rate.

It was concluded that the maximum value is obtained at the point $p1$, which is located near the tongue region at $0.4Q_d$. The minimum value is obtained at $p6$, which is located far from the tongue. In general, the amplitude of pressure at monitoring points decreases from the point near the tongue region along the impeller rotation direction. Its minimum value is achieved at the point located farthest from the tongue.

3.5. Pressure Coefficient Distribution. Figure 11 presents pressure distribution on the center plane under various flow rates. The pressure coefficient is defined as follows:

$$c_{p1} = \frac{p - p_{\mathrm{ref}}}{0.5\rho u^2}, \tag{3}$$

where p stands for static pressure, p_{ref} stands for the reference pressure (1 atm), and u stands for impeller circumferential velocity. In general, along the direction from the impeller inlet to the volute outlet, the pressure presents a trend of gentle and continuous increase. The minimum pressure is obtained at the inlet of the impeller, and the maximum pressure is obtained at the outlet of the pump. In addition, the pressure in the pump is larger at a small flow rate. As the flow increases, the pressure gradually decreases. At partial flow rate, low-pressure regions are observed clearly at the leading edge, and pressure coefficient distribution is nonuniform at the inlet of the impeller passages, especially at $0.4Q_d$. With the increase of the flow rate, the pressure in the impeller passage increases gently. At the

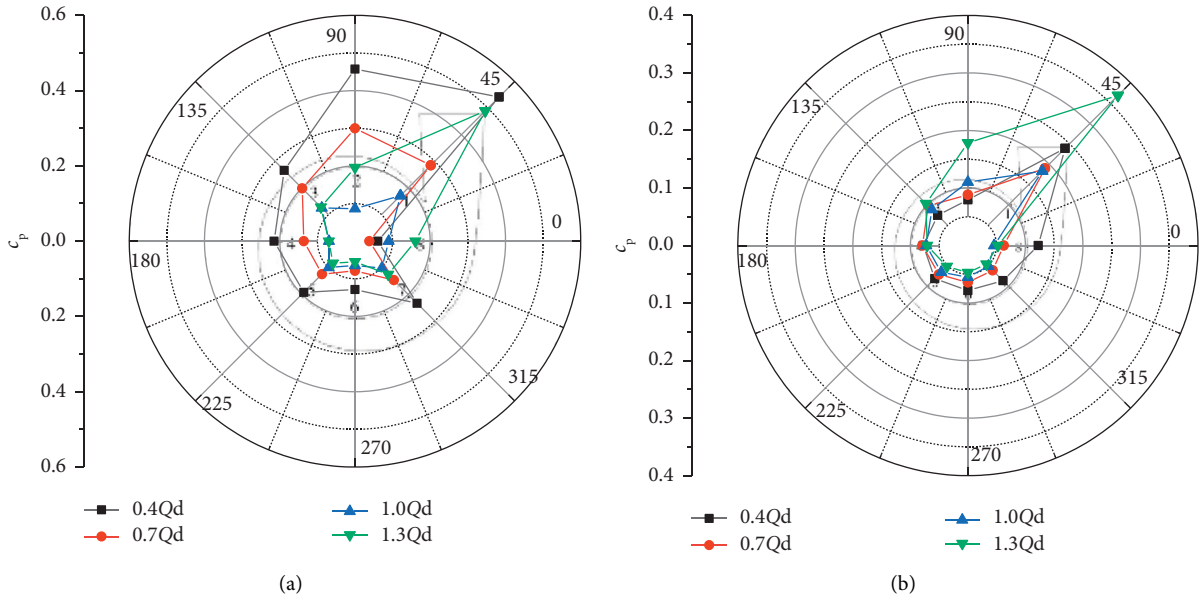

FIGURE 13: Pressure amplitude distribution under f_{BPF} and $2f_{BPF}$. (a) Pressure amplitude under f_{BPF} and (b) pressure amplitude under $2f_{BPF}$.

design flow rate, the pressure distribution is evenly distributed and increases gradually from inlet to outlet of the impeller. The pressure difference is relatively small between both sides of the impeller passages which reveals a good flow situation. As the flow rate increase to $1.3Q_d$, the pressure amplitude decreases significantly, and the distribution is still relatively uniform. While enlarged low-pressure areas are captured at the trailing edge in one impeller rotating period with the increase of the flow rate. The interaction between the low-pressure areas near the trailing edge and the high-pressure area in the volute and the strong rotor-stator interaction may be the major reason for the increase of pressure fluctuation in the frequency domain near the tongue region.

Figure 14 presents the pressure distribution of blade surfaces in impeller passage *A*, which is shown in Figure 3. *L* stands for the relative length of the blade. It was found that the pressure coefficient on the pressure side is larger than that on the suction side. In general, the pressure increases gradually along the direction from the impeller inlet to the impeller outlet.

The maximum pressure value is achieved near the region at the impeller outlet for the pressure side (PS) and suction side (SS). However, the pressure is decreased to a certain extent at the impeller outlet, which is caused by the low-pressure region near.

Trailing edge (TE). At $0.4Q_d$, the pressure coefficient on the PS and SS is the worst and nonuniform. Besides, the intersections are found on both sides of the blade surfaces. The pressure coefficient on PS is enlarged significantly after about $0.7L$, which is in good agreement with Figure 11(a). Large adverse pressure gradient and pressure difference on both sides of the blade surfaces are easy to generate the flow separation and secondary flow, which finally results in the unsteady internal flow situation. As

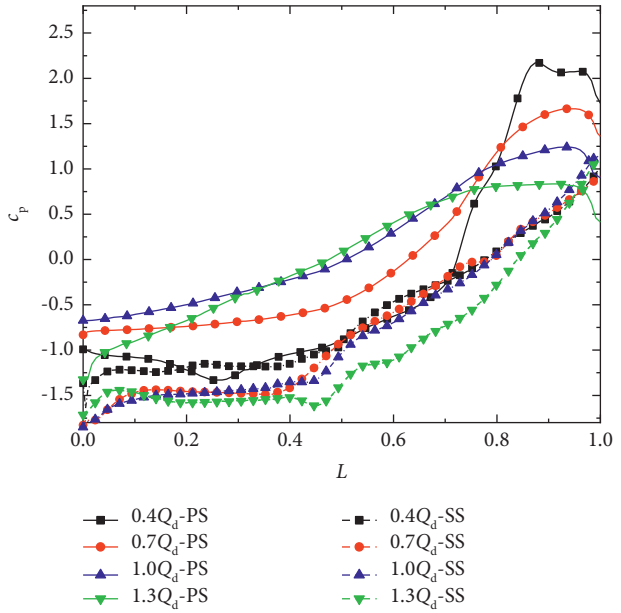

FIGURE 14: Pressure coefficient distribution of blade surfaces on the center plane.

the flow rate increases to the design flow rate, pressure increases slightly and the pressure difference on the PS and SS is reduced. Smooth pressure changes on both sides of the flow passage indicate a good internal flow situation. At $1.3Q_d$, the pressure on the PS increases slowly, and the pressure near the outlet of the flow channel decreases. However, the pressure on the SS is significantly reduced. In addition, it was also found that the low-pressure area at the trailing edge of the blade tends to expand as the flow rate increases.

4. Conclusions

In the present work, the numerical calculation is performed for the three-dimensional centrifugal pump in order to investigate the characteristics of pressure fluctuation in a centrifugal pump at design and off-design flow rates. The numerical calculation results are in good agreement with the experimental data, which proves the reliability of the calculation results. The conclusions obtained from the numerical simulations are as follows:

(1) The periodicity of pressure fluctuation is captured in the time-domain distribution, and the distribution of pressure fluctuation appears irregular under a small flow rate. The average pressure at the impeller outlet increases rapidly at a small flow rate from the tongue along the impeller rotation direction, while the pressure distribution is the opposite at a large flow rate.

(2) The dominant frequency is clearly obtained under various flow rates. The amplitude of pressure fluctuation is minimum at the design flow rate, and increases at the off-design flow rate, especially at a small flow rate. In addition, as the flow rate decreases, the pressure distribution on both sides of the flow channel becomes worse, which is mainly reflected in the suction side of the blade.

(3) The distribution of frequency spectra is nonuniform at the impeller outlet circumferential direction. Its amplitude decreases along the impeller rotation direction near the tongue region, and a minimum value are achieved near the region far away from the tongue.

Nomenclature

c_p: Pressure fluctuation coefficient
D_0: Inlet diameter of the impeller
D_1: Outlet diameter of the impeller
f_n: Impeller rotating frequency
g: Gravity
H: Pressure head
φ: Pressure head coefficient
L: Relative length of the blade
n: Rotating speed
p: Static pressure
p_{ref}: Reference pressure
Q_d: Design flow rate
u: Impeller circumferential velocity
Z: Number of blades

Data Availability

The data used to support the findings of this study are available from the corresponding author upon request.

Conflicts of Interest

The authors declare no conflicts of interest.

Acknowledgments

This research was supported by the National Natural Science Foundation of China (51976198), the Key Research and Promotion Special Funding Project of Henan Province (202102210286 and 212102210324), the Key Scientific Research Projects of the Higher Education Institutions of Henan Province (21A460004), and Research Foundation for Talented Scholars of Henan Institute of Technology (KQ1862 and KQ1861).

References

[1] Y. L. Zhang, Z. C. Zhu, Y. N. Sheng, B. L. Cui, and Y. Li, "Experimental study on a prototype centrifugal pump with open impeller during stopping period," *International Journal of Fluid Mechanics Research*, vol. 43, no. 1, pp. 18–27, 2016.

[2] Y. Y. Liu, Y. R. Li, and L. Q. Wang, "Experimental and theoretical studies on the pressure fluctuation of an internal gear pump with a high pressure," *Proceedings of the Institution of Mechanical Engineers-Part C: Journal of Mechanical Engineering Science*, vol. 233, no. 3, pp. 987–996, 2019.

[3] X. P. Chen, Z. C. Zhu, H.-S. Dou, and Y. Li, "Large eddy simulation of energy gradient field in a centrifugal pump impeller," *Proceedings of the Institution of Mechanical Engineers-Part C: Journal of Mechanical Engineering Science*, vol. 233, no. 11, pp. 4047–4057, 2019.

[4] L. L. Zheng, X. P. Chen, W. Zhang et al., "Investigation on characteristics of pressure fluctuation in a centrifugal pump with clearance flow," *Journal of Mechanical Science and Technology*, vol. 34, no. 9, pp. 3657–3666, 2020.

[5] M. Liu, L. Tan, and S. L. Cao, "Cavitation-vortex-turbulence interaction and one-dimensional model prediction of pressure for hydrofoil ALE15 by large eddy simulation," *Journal of Fluids Engineering*, vol. 141, no. 2, Article ID 021103, 2019.

[6] W. H. Sun and L. Tan, "Cavitation-vortex-pressure fluctuation interaction in a centrifugal pump using bubble rotation modified cavitation model under partial load," *Journal of Fluids Engineering*, vol. 142, no. 5, Article ID 051206, 2020.

[7] W. Y. Xiao and L. Tan, "Design method of controllable velocity moment and optimization of pressure fluctuation suppression for a multiphase pump," *Ocean Engineering*, vol. 220, Article ID 108402, 2021.

[8] Y. Song, Z. Y. Yu, G. T. Shi, and X. B. Liu, "Influence of impeller staggered arrangement on radial force and pressure fluctuation for a double-suction centrifugal pump," *Advances in Mechanical Engineering*, vol. 10, no. 6, Article ID 168781401878146, 2018.

[9] W. W. Zhang, Z. Y. Yu, and B. S. Zhu, "Influence of tip clearance on pressure fluctuation in low specific speed mixed-flow pump passage," *Energies*, vol. 10, no. 2, p. 148, 2017.

[10] Y. Long, D. Z. Wang, J. L. Yin, and Y. Y. Hu, "Experimental investigation on the unsteady pressure pulsation of reactor coolant pumps with non-uniform inflow," *Annals of Nuclear Energy*, vol. 110, pp. 501–510, 2017.

[11] J. Gonzalez, J. Fernández, E. Blanco, and C. Santolaria, "Numerical simulation of the dynamic effects due to impeller-volute interaction in a centrifugal pump," *Journal of Fluids Engineering*, vol. 124, no. 2, pp. 348–355, 2002.

[12] L. Bai, L. Zhou, C. Han, Y. Zhu, and W. Shi, "Numerical study of pressure fluctuation and unsteady flow in a centrifugal pump," *Processes*, vol. 7, no. 6, p. 354, 2019.

[13] C. Wang, X. He, W. Shi, X. Wang, X. Wang, and N. Qiu, "Numerical study on pressure fluctuation of a multistage centrifugal pump based on whole flow field," *AIP Advances*, vol. 9, no. 3, Article ID 035118, 2019.

[14] Y. B. Liu and L. Tan, "Spatial-temporal evolution of tip leakage vortex in a mixed-flow pump with tip clearance," *Journal of Fluids Engineering*, vol. 141, no. 8, Article ID 081302, 2019.

[15] Y. B. Liu and L. Tan, "Theoretical prediction model of tip leakage vortex in a mixed flow pump with tip clearance," *Journal of Fluids Engineering*, vol. 142, no. 2, Article ID 021203, 2020.

[16] Y. D. Han and L. Tan, "Dynamic mode decomposition and reconstruction of tip leakage vortex in a mixed flow pump as turbine at pump mode," *Renewable Energy*, vol. 155, pp. 725–734, 2020.

[17] Z. X. Gao, W. R. Zhu, L. Lu, J. Deng, J. G. Zhang, and F. Wuang, "Numerical and experimental study of unsteady flow in a large centrifugal pump with stay vanes," *Journal of Fluids Engineering*, vol. 136, no. 7, Article ID 071101, 2014.

[18] Y. Song, H. Fan, W. Zhang, and Z. Xie, "Flow characteristics in volute of a double-suction centrifugal pump with different impeller arrangements," *Energies*, vol. 12, no. 4, p. 669, 2019.

[19] R. Spence and J. Amaral-Teixeira, "Investigation into pressure pulsations in a centrifugal pump using numerical methods supported by industrial tests," *Computers & Fluids*, vol. 37, no. 6, pp. 690–704, 2008.

[20] F. Y. Jin, Z. F. Yao, D. M. Li, R. F. Xiao, F. J. Wang, and C. L. He, "Experimental investigation of transient characteristics of a double suction centrifugal pump system during starting period," *Energies*, vol. 12, no. 21, p. 4135, 2019.

[21] N. Zhang, M. Yang, B. Gao, Z. Li, and D. Ni, "Experimental investigation on unsteady pressure pulsation in a centrifugal pump with special slope volute," *Journal of Fluids Engineering*, vol. 137, no. 6, Article ID 061103, 2015.

[22] B. Gao, N. Zhang, Z. Li, D. Ni, and M. G. Yang, "Influence of the blade trailing edge profile on the performance and unsteady pressure pulsations in a low specific speed centrifugal pump," *Journal of Fluids Engineering*, vol. 138, no. 5, Article ID 051106, 2016.

[23] B. Gao, P. M. Guo, N. Zhang, Z. Li, and M. G. Yang, "Unsteady pressure pulsation measurements and analysis of a low specific speed centrifugal pump," *Journal of Fluids Engineering*, vol. 139, no. 7, Article ID 071101, 2017.

[24] Z. J. Jin, Z. X. Gao, M. Zhang, and J. Y. Qian, "Pressure drop analysis of pilot-control globe valve with different structural parameters," *Journal of Fluids Engineering*, vol. 139, no. 9, Article ID 091102, 2017.

[25] J. Yan, Z. Zuo, W. Guo, H. Hou, X. Zhou, and H. Chen, "Influences of wear-ring clearance leakage on performance of a small-scale pump-turbine," *Proceedings of the Institution of Mechanical Engineers-Part A: Journal of Power and Energy*, vol. 234, no. 4, pp. 454–469, 2020.

[26] Z. F. Xu, F. Y. Kong, L. Tang, M. W. Liu, J. Q. Wang, and N. Qiu, "Effect of blade thickness on internal flow and performance of a plastic centrifugal pump," *Machines*, vol. 10, no. 1, p. 61, 2022.

[27] Y. B. Liu, L. Tan, M. Liu, Y. Hao, and Y. Xu, "Influence of prewhirl angle and axial distance on energy performance and pressure fluctuation for a centrifugal pump with inlet guide vanes," *Energies*, vol. 10, no. 5, p. 695, 2017.

[28] H. S. Dou, W. Jiang, Y. L. Zhang, Z. C. Zhu, B. L. Cui, and Y. Li, "Flow instability in a centrifugal pump based on energy gradient theory," *Transactions of the Chinese Society for Agricultural Machinery*, vol. 45, pp. 88–92, 2014.

[29] R. F. Kuang, Z. M. Zhang, S. L. Wang, and X. P. Chen, "Effect of hub inclination angle on internal and external characteristics of centrifugal pump impellers," *AIP Advances*, vol. 11, no. 2, Article ID 025043, 2021.

[30] R. Barrio, E. Blanco, J. Parrondo, J. González, and J. Fernández, "The effect of impeller cutback on the fluid-dynamic pulsations and load at the blade-passing frequency in a centrifugal pump," *Journal of Fluids Engineering*, vol. 130, no. 11, pp. 859–870, 2008.

[31] R. Barrio, J. Parrondo, and E. Blanco, "Numerical analysis of the unsteady flow in the near-tongue region in a volute-type centrifugal pump for different operating points," *Computers & Fluids*, vol. 39, no. 5, pp. 859–870, 2010.

[32] N. Zhang, M. G. Yang, B. Gao, Z. Li, and D. Ni, "Investigation of rotor-stator interaction and flow unsteadiness in a low specific speed centrifugal pump," *Strojniški vestnik-Journal of Mechanical Engineering*, vol. 62, no. 1, pp. 21–31, 2016.